Catching gas with droplets

Modelling and simulation of a diffusion-reaction process

Simon van Mourik[1], Yves van Gennip[2], Mark Peletier[2], Andriy Hlod[2], Vadim Shcherbakov[3], Peter in 't Panhuis[2], Erwin Vondenhoff[2], Pieter Eendebak[4], Jan Bouwe van den Berg[5]

Abstract

The packaging industry wants to produce a foil for food packaging purposes, which is transparent and lets very little oxygen pass. To accomplish this they add a scavenger material to the foil which reacts with the oxygen that diffuses through the foil. We model this process by a system of partial differential equations: a reaction-diffusion equation for the oxygen concentration and a reaction equation for the scavenger concentration. A probabilistic background of this model is given and different methods are used to get information from the model. Homogenization theory is used to describe the influence of the shape of the scavenger droplets on the oxygen flux, an argument using the Fourier number of the foil leads to insight into the dependency on the position of the scavenger and a method via conformal mappings is proposed to find out more about the role of the size of the droplet. Also simulations with *Mathematica* were done, leading to comparisons between different placements and shapes of the scavenger material in one- and two-dimensional foils.

Keywords: pde modeling, chemical reaction, simulation, homogenization, conformal mapping, Fourier number

4.1 Introduction

In the food packaging industry people are interested in developing materials that can shield food from certain gasses, like oxygen. If too much oxygen comes into contact with the food, the rotting process will set in. For a lot of food the tolerable oxygen concentration is in the order of ten parts per million, as listed in figure 4.1. An additional demand on the packaging foil is transparency, since

1: Universiteit Twente, 2: Technische Universiteit Eindhoven, 3: CWI, 4: Universiteit Utrecht, 5: Vrije Universiteit Amsterdam

customers like to see the food before they buy it. As a solution satisfying both demands DSM considers a polymer sheet which contains droplets of a material that reacts with oxygen, the so called scavenger material. Through reaction with this material the concentration of oxygen in the foil decreases and the flux of oxygen through the packaging material is less than it would be in the absence of scavenger droplets.

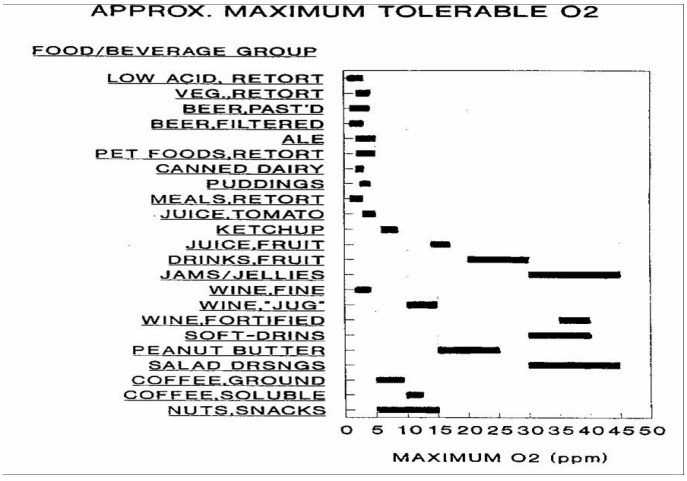

Figure 4.1: Tolerable oxygen concentrations for different types of food.

The question posed by DSM to the *55th European Study Group Mathematics With Industry* was twofold. Firstly they asked the participants to model the diffusion of oxygen gas through a foil containing scavenger droplets. Since DSM is mainly interested in the flux of oxygen through the foil and not so much in the specifics of the diffusion inside the foil, the hope was that the Study Group would come up with a model of the full three-dimensional process, rooted in physics, which could then be simplified to a one-dimensional effective model describing the oxygen flux across the foil. One difficulty in describing the process at hand is the fact that due to reaction with oxygen the scavenger concentration decreases with time.

Secondly DSM was interested in predictions of this model about the influence of the concentration, shape and size of the scavenger droplets on the oxygen flux. The production process is such that after the droplets are added to the packaging material, the foil can be stretched in one of two ways, either uniaxial or biaxial. In the former case the stretching is done in one direction in the plane of the foil, which results in cigar-shaped droplets, in the latter case the stretching takes place in two perpendicular directions in the plane of the foil, resulting in pancake-shaped droplets. In the absence of stretching the droplets remain spherical in first approximation. Furthermore, during addition of the scavenger material, the amount of added scavenger can be controlled as can the size of the added droplets, but the spatial placement of droplets in the

foil cannot. Thus a homogeneous spread of droplets in the material should be assumed.

The problem owners from DSM already came up with a one-dimensional model of the process themselves, which they hoped could be either validated or improved upon during the Study Group. This model consists of a reaction-diffusion equation for the oxygen concentration $\tilde{c}(x,t)$ coupled to a reaction equation for the concentration of scavenger material $\tilde{s}(x,t)$:

$$\frac{\partial \tilde{c}(x,t)}{\partial t} = D\frac{\partial^2 \tilde{c}(x,t)}{\partial x^2} - \kappa_c\, \tilde{s}(x,t)^\alpha \tilde{c}(x,t)^\beta, \tag{4.1a}$$

$$\frac{\partial \tilde{s}(x,t)}{\partial t} = -\kappa_s\, \tilde{s}(x,t)^\alpha \tilde{c}(x,t)^\beta, \tag{4.1b}$$

where D is the diffusion coefficient for oxygen in the polymer foil, κ_c is the reaction rate of oxygen and κ_s is the reaction rate of scavenger material. All these coefficients as well as α and β are taken to be constant in space and time. The values of these constants are fully determined by the properties of the foil, the scavenger material and oxygen and are not dependent on the placement, size or shape of the scavenger droplets. Multiplying equation (4.1a) by κ_s and equation (4.1b) by κ_c and subsequently re-scaling the oxygen and scavenger concentrations as $c(x,t) := \kappa_s \tilde{c}(x,t)$ and $s(x,t) := \kappa_c \tilde{s}(x,t)$ leads to the following system of partial differential equations, where now the reaction constant $\kappa := \kappa_c^{-\alpha+1}\kappa_s^{-\beta+1}$ is the same in both equations:

$$\frac{\partial c(x,t)}{\partial t} = D\frac{\partial^2 c(x,t)}{\partial x^2} - \kappa\, s(x,t)^\alpha c(x,t)^\beta, \tag{4.2a}$$

$$\frac{\partial s(x,t)}{\partial t} = -\kappa\, s(x,t)^\alpha c(x,t)^\beta. \tag{4.2b}$$

According to DSM, experimental results indicate that $\alpha \approx \frac{5}{3}$ and $\beta \approx 1$. However in our treatment of this model we will often take both these constants to be 1 for simplicity. The system of equations (4.2a) and (4.2b) will be called the *DSM model* from here on.

Both questions DSM asked the Study Group sparked a lot of different initiatives which led to some useful insights into the problem. In this report the different approaches to the proposed problems are discussed and practical results useful for DSM as well as possible new directions for research will be given. The setup for this report will be as follows. In section 4.2 a probabilistic model for the physics on the micro scale is given and the relation between this model and the DSM model of partial differential equations is discussed. Section 4.3 applies the theory of homogenization to a three dimensional generalization of the DSM model with constant scavenger concentration. This approach results in, among other things, a limit problem in which the influence of the shape of the droplet is felt via the first eigenvalue of the Laplacian on a cube with a droplet shaped cavity. In section 4.4 the effects of the position of the scavenger are investigated analytically. The final analytical approach which was undertaken comprises the use of conformal mappings to transform the stationary

problem, i.e. the Laplace equation, on an infinite strip with a rectangular hole to a similar problem on the complex half plane and can be found in section 4.5. The strip with the rectangular hole models the polymer foil with a rectangular droplet of scavenger material in it. The last of the approaches proposed during the Study Group week that will be discussed in this report is the numerical one and can be found in sections 4.6 and 4.7. Simulations in *Mathematica* of the DSM model in one and two space dimensions were made, leading to some new insights in the effects of placement and shape of the scavenger material on the oxygen flux through the foil. In the final section 4.8 the results and conclusion that we think are of greatest interest to DSM, will be restated.

4.2 Probabilistic approach

In this section we propose a possible idealized stochastic microscopic model of catching oxygen by droplets. The model is based on the following three assumptions regarding the chemistry and the physics of the phenomena.

- **A1**: Oxygen molecules move *independently*. The free individual dynamics of any oxygen molecule is simple diffusion that has no preferential directions.
- **A2**: Oxygen molecules interact with droplets *independently* of each other.
- **A3**: When a particle (molecule) hits a droplet, then there is a chance that it can be annihilated. If the reaction takes place, then it affects the droplet too. Namely, it makes the droplet's catching properties worse. Therefore the effectiveness of the reaction process decreases in time.

As operator space, we take the lattice $\mathbf{Z}^d$, where $\mathbf{Z}$ is a set of integers and d can be $1, 2$ or 3. For definiteness we assume $d = 1$ in the sequel. Assumption **A1** suggests that we can model the oxygen molecules by independent simple symmetric random walks $\{x_i(t) \in \mathbf{Z},\, t \geq 0,\, i = 1, 2, \ldots\}$. Let us explain informally what a simple random walk on the lattice is. One can think of a particle that moves on $\mathbf{Z}$ as follows. Assume that a particle is at point $k \in \mathbf{Z}$ at time $t \geq 0$. The particle sits at this point for a random time t_k (which is an exponentially distributed random variable with parameter $\lambda > 0$), then it jumps to either site $k-1$ or $k+1$ chosen with probability $1/2$. It occupies the new location for another exponentially distributed random time (which is independent of t_k), and jumps again to one of the nearest neighbors chosen equally likely and so on. Formally, a simple symmetric random walk $x(t)$, $t \geq 0$, on the lattice $\mathbf{Z}$ is a continuous time Markov chain whose dynamic is specified by the following infinitesimal probabilities

$$\mathsf{P}\left\{x(t+\delta t) = y | x(t) = x\right\} = \begin{cases} D\delta t/2 + O(\delta t), & \text{if } |x-y| = 1, \\ 1 - D\delta t + O(\delta t), & \text{if } x = y, \\ 0, & \text{if } |x-y| > 1, \end{cases}$$

where $x, y \in \mathbf{Z}$, D is a diffusion coefficient and $O(\delta t) \to 0$ as $\delta t \to 0$. D specifies the intensity of jumps and it is equal to λ^{-1}.

The random walks interact with a random medium modelling scavenger droplets. In the DSM model the distribution of the scavenger material is specified by its concentration at every point inside the foil. In our model we introduce a system of independent nonnegative integer valued random processes $\{\eta_k(t),\, k \in \mathbf{Z},\, t \geq 0\}$ which are interpreted as amounts of scavenger material at the lattice points at time t.

Let us describe an interaction between particles and droplets. Denote by $\xi_k(t)$ a number of particles at point $k \in \mathbf{Z}$ at time t. Consider a point k such that $\xi_k(t) > 0$ and $\eta_k(t) > 0$. Within the time interval $[t, t+\delta t)$ any oxygen molecule at this point can react with a droplet with probability $F(\eta_k(t))\delta t + O(\delta t)$, where $O(\delta t) \to 0$ as $\delta t \to 0$. Here $F(\cdot)$ is some nonnegative function, such that $F(0) = 0$. With probability $1 - F(\eta_k(t))\delta t + O(\delta t)$ the molecule does not react. As a result of the reaction the oxygen molecule and a certain amount of scavenger material annihilate each other, therefore $\xi_k(t) \to \xi_k(t) - 1$ and $\eta_k(t) \to \eta_k(t) - 1$ respectively. When all the scavenger material is reacted away, then subsequently the oxygen molecules diffuse passively through without being affected.

Let us compute the probability of the event that at least one of the oxygen molecules reacts at point k during the time interval $[t, t+\delta t)$. Assumption **A2** yields that the probability of the event that exactly $0 < j < m = \min(\xi_k(t),\, \eta_k(t))$ molecules react during time interval $[t,\, \delta t)$ is given by

$$\binom{m}{j} (F(\eta_k(t))\delta t + O(\delta t))^j (1 - F(\eta_k(t))\delta t + O(\delta t))^{m-j}$$

and it is negligible in comparison with $F(\eta_k(t))\delta t$ as δt goes to 0. Therefore the probability of the event that at least one molecule reacts during the time interval $[t, t+\delta t)$ is equal to

$$\xi_k(t) F(\eta_k(t))\delta t + O(\delta t), \tag{4.3}$$

and it is the probability of the event that exactly one of the molecules reacts within the same time interval. The coefficient in front of δt, i.e. $\xi_k(t)F(\eta_k(t))$ is, by definition, the total reaction rate at point k at time t.

Back to the continuum equations

In this section we show the connection between the microscopic probabilistic model and the following system of partial differential equations

$$\frac{\partial c(x,t)}{\partial t} = D\frac{\partial^2 c(x,t)}{\partial x^2} - F(s(x,t))c(x,t), \tag{4.4a}$$

$$\frac{\partial s(x,t)}{\partial t} = -F(s(x,t))c(x,t). \tag{4.4b}$$

In particular, if $F(x) = \kappa x^{5/3}$, then we get the DSM model. We would like to highlight the main idea and will not go into many technical details. The idea is to consider the stochastic system at points $k(\varepsilon) \sim [x/\varepsilon]$, where $x \in \mathbf{R}$, after time $t(\varepsilon) = t/\varepsilon^2$ and then pass to the limit $\varepsilon \to 0$. It is a so-called hydrodynamic limit in the standard terminology of statistical physics. Points $k(\varepsilon)$ are microscopic points, $t(\varepsilon)$ is microscopic time. Respectively, continuous point x is called a macroscopic one and t is the macroscopic time. The reaction rates should be rescaled respectively, since the impact of the reaction at any microscopic point should be negligible at macroscopic scale, but the effect of the reaction is visible in a continuum domain with positive volume. Namely, we put the reaction rate equal to $\varepsilon^2 F(\cdot)$ (in a few lines this choice will become clear). Formally, the pair of random processes $(\xi(t/\varepsilon^2), \eta(t/\varepsilon^2))$ forms a Markov process with the state space $S = \{(\xi, \eta) \in (\mathbf{Z}_+ \cup \{0\})^\infty \times (\mathbf{Z}_+ \cup \{0\})^\infty\}$ and with the following infinitesimal operator

$$\begin{aligned} G_\varepsilon f(\xi,\eta) = {} & \varepsilon^{-2} D \sum_k \left(f\left(\xi + e_{k+1} - e_k, \eta\right) - f\left(\xi,\eta\right)\right) \xi_k \\ & + \varepsilon^{-2} D \sum_k \left(f\left(\xi + e_{k-1} - e_k, \eta\right) - f\left(\xi,\eta\right)\right) \xi_k \\ & + \varepsilon^{-2} \sum_k \left(f\left(\xi - e_k, \eta - e_k\right) - f\left(\xi,\eta\right)\right) \xi_k F(\eta_k)\varepsilon^2 \end{aligned} \tag{4.5}$$

where $e_k \in \mathbf{Z}^\infty$ are infinite dimensional vectors with all zero components except the kth, which are equal to 1. Existence of this process can be proved by the general methods of the theory of interacting particle systems, we refer to [5] for more details. The factor ε^{-2} in front of the sums manifests the fact that we speed up the process time. Obviously, in the third sum it cancels out with its reciprocal in the reaction term $\xi_k F(\eta_k)\varepsilon^2$. For any $\varepsilon > 0$ consider a random process

$$J_\varphi^{(\varepsilon)}(t) = \varepsilon \sum_{k \in \mathbf{Z}} \varphi(\varepsilon k) \xi_k \left(t/\varepsilon^2\right),$$

where $\varphi : \mathbf{R} \to \mathbf{R}$ is an integrable bounded function (test function). $J_\varphi^{(\varepsilon)}(t)$ is nothing else but an integral of the function φ with respect to the measure

$$\mu_t^\varepsilon = \varepsilon \sum_{k \in \mathbf{Z}} \xi_k \left(t/\varepsilon^2\right) \delta_{\{\varepsilon k\}}(\cdot), \tag{4.6}$$

where $\delta_{\{x\}}(\cdot)$ is a delta function at point $x \in \mathbf{R}$. It follows from the theory of Markov processes that we can write

$$J_\varphi^{(\varepsilon)}(t) = J_\varphi^{(\varepsilon)}(0) + \int_0^t G_\varepsilon J_\varphi^{(\varepsilon)}(s) ds. \tag{4.7}$$

Direct computations show that

$$\begin{aligned} G_\varepsilon J_\varphi^{(\varepsilon)}(s) &= \varepsilon^{-1} D \sum_{k\in\mathbf{Z}} \left(\varphi(k\varepsilon+\varepsilon)-\varphi(k\varepsilon)\right)\xi_k\left(s/\varepsilon^2\right) \\ &+ \varepsilon^{-1} D \sum_{k\in\mathbf{Z}} \left(\varphi(k\varepsilon-\varepsilon)-\varphi(k\varepsilon)\right)\xi_k\left(s/\varepsilon^2\right) \\ &+ \sum_k \left(\varphi(k\varepsilon-\varepsilon)-\varphi(k\varepsilon)\right)\xi_k\left(s/\varepsilon^2\right) F(\eta_k\left(s/\varepsilon^2\right)). \end{aligned}$$

Assuming that function φ is smooth enough we can use the Taylor expansion and obtain that

$$\begin{aligned} G_\varepsilon J_\varphi^{(\varepsilon)}(s) &= \varepsilon D \sum_{k\in\mathbf{Z}} \varphi''(k\varepsilon)\xi_k\left(s/\varepsilon^2\right) - \varepsilon \sum_{k\in\mathbf{Z}} \varphi'(k\varepsilon)\xi_k\left(s/\varepsilon^2\right) F\left(\eta_k\left(s/\varepsilon^2\right)\right) \\ &+ R_\varphi(\varepsilon), \end{aligned}$$

where $R_\varphi(\varepsilon) \to 0$ in probability as $\varepsilon \to 0$. Substituting it into the equation (4.7) we obtain

$$\begin{aligned} \varepsilon \sum_{k\in\mathbf{Z}} \varphi(\varepsilon k)\xi_k\left(t/\varepsilon^2\right) - \varepsilon \sum_{k\in\mathbf{Z}} \varphi(\varepsilon k)\xi_k(0) &= \varepsilon D \int_0^t \sum_{k\in\mathbf{Z}} \varphi''(k\varepsilon)\xi_k\left(s/\varepsilon^2\right) ds \\ &- \varepsilon \int_0^t \sum_{k\in\mathbf{Z}} \varphi'(k\varepsilon)\xi_k\left(s/\varepsilon^2\right) F(\eta_k\left(s/\varepsilon^2\right))ds + R_\varphi(\varepsilon). \end{aligned} \tag{4.8}$$

Repeating the same arguments for a random process

$$\varepsilon \sum_{k\in\mathbf{Z}} \psi(\varepsilon k)\eta_k\left(t/\varepsilon^2\right)$$

which is an integral of test function ψ with respect to another measure

$$\nu_t^{(\varepsilon)} = \varepsilon \sum_{k\in\mathbf{Z}} \eta_k\left(t/\varepsilon^2\right)\delta_{\{\varepsilon k\}}(\cdot),$$

we obtain that

$$\begin{aligned} \varepsilon \sum_{k\in\mathbf{Z}} \psi(\varepsilon k)\eta_k\left(t/\varepsilon^2\right) - \varepsilon \sum_{k\in\mathbf{Z}} \psi(\varepsilon k)\eta_k\left(0\right) &\\ = -\varepsilon \int_0^t \sum_{k\in\mathbf{Z}} \psi'(k\varepsilon)\xi_k\left(s/\varepsilon^2\right) F(\eta_k\left(s/\varepsilon^2\right))ds + R_\psi(\varepsilon), & \end{aligned} \tag{4.9}$$

where $R_\psi(\varepsilon) \to 0$ in probability as $\varepsilon \to 0$. So, informally, we can conclude that the pair $(\xi(t/\varepsilon^2), \eta(t/\varepsilon^2))$ "mimics" a weak solution of the system of equations (4.4a) and (4.4b). To see this, one should replace in equations (4.8) and (4.9)

the random processes $\xi\left(\tau/\varepsilon^2\right)$ and $\eta(\tau/\varepsilon^2)$ by functions $c(x,\tau)$ and $s(x,\tau)$ respectively, and the sums over k should be replaced by integrals. If functions ($c(x,\tau)$ and $s(x,\tau)$) satisfy such integral equations for any smooth enough finitely supported functions φ and ψ, then, by definition, they form a weak solution of the system of equations (4.4a) and (4.4b).

The reasoning above can be placed in a rigorous setting of the modern theory of hydrodynamic limits for interacting particle systems [4]. Using the general methods of this theory it is possible to prove that the Markov process $(\xi(t/\varepsilon^2), \eta(t/\varepsilon^2))$, $t \geq 0$, converges in some rigorous sense to a weak solution of the system of equations (4.4a)–(4.4b) as $\varepsilon \to 0$. It can be shown (using the methods of the theory of partial differential equations) that there exists a unique weak solution in this case. Then, it remains to note that any strong solution is a weak solution. Hence, uniqueness of the strong solution implies that the obtained weak solution is in fact a strong solution of the system of equations (4.4a)–(4.4b).

Experimental results of DSM show that the equation for the oxygen concentration $c(t,x)$ should be linear in $c(t,x)$. We have just shown that our microscopic probabilistic model leads to this type of equations. This is determined by the fact that the total reaction rate (see equation (4.3)) is linear in the number of oxygen molecules at a point due to Assumption **A2**.

We would suggest a simulation study of the proposed stochastic model. In this study the described particle system can be simulated in a finite lattice volume with certain boundary conditions and the droplet shapes can be taken into account. The parameters of the simulated model should be specified in collaboration with DSM in order to have a plausible approximation to the real situation.

4.3 Homogenization

In this section we study the limit of small length size and derive a description in terms of homogenized quantities.

The starting point for our discussion is the system of equations

$$c_t = D\Delta c - kcs \qquad \text{for } x \in \Omega,\ t > 0 \tag{4.10a}$$

$$s_t = -kcs \qquad \text{for } x \in \Omega,\ t > 0 \tag{4.10b}$$

$$c = c_b \qquad \text{for } t > 0 \text{ and } x \in \partial\Omega \tag{4.10c}$$

$$(c, s) = (c_i, s_i) \qquad \text{for } t = 0 \text{ and } x \in \Omega. \tag{4.10d}$$

Here Ω is a domain in $\mathbb{R}^n$ representing the foil; c_b is a given boundary value function, c_i and s_i are the initial data for the oxygen and scavenger concentrations, and k and D are reaction and diffusion parameters. The assumption that the scavenger is contained in small inclusions is encoded in the initial datum s_i.

The relevant dimensionless parameter that indicates whether the problem is diffusion- or reaction-dominated is

$$\alpha := \frac{D}{\varepsilon^2 k S}$$

where ε is the typical microscopic length scale (the distance between scavenger inclusions) and S is a typical scale of s. If this number is large, then the diffusion is fast enough to homogenize differences on length scales ε; if it is small, then the fast reaction creates large local variations of c.

Diffusion-dominated

If α is large, then the concentration c varies little between regions with and without scavenger; one can directly write down the homogenized problem (cf. [2]),

$$c_t = D\Delta c - kcs \qquad \text{for } x \in \Omega,\ t > 0 \tag{4.11a}$$
$$s_t = -kcs \qquad \text{for } x \in \Omega,\ t > 0 \tag{4.11b}$$
$$c = c_b \qquad \text{for } t > 0 \text{ and } x \in \partial\Omega \tag{4.11c}$$
$$(c, s) = (\overline{c_i}, \overline{s_i}) \qquad \text{for } t = 0 \text{ and } x \in \Omega, \tag{4.11d}$$

where now $\overline{c_i}$ and $\overline{s_i}$ are locally averaged (macroscopic) concentrations. Note that in this problem the length scale of the scavenger inclusions no longer appears (it is involved indirectly in determining $\overline{s_i}$).

Reaction-dominated

On the other hand, if α is small, then the reaction forces the concentration of c to zero wherever s is non-zero.

In the limit $\alpha \to 0$ problem (4.10) converges to a Stefan problem:

$$c_t = D\Delta c \qquad \text{in } \{c > 0\} \tag{4.12a}$$
$$c = c_b \qquad t > 0,\ x \in \partial\Omega \tag{4.12b}$$
$$v_n = -\frac{1}{s_i}\frac{\partial c}{\partial n} \qquad \text{on } \partial\{c > 0\} \setminus \partial\Omega \tag{4.12c}$$

where n is the outward normal to $\{c > 0\}$ and v_n is the velocity of the interface $\partial\{c > 0\}$. Recall that s_i is the initial s-concentration; in the limit the concentration of s at any point x does not change until the interface reaches x. (This convergence result is proved in [1] for one dimension). The domain thus splits in two parts: one where $ks = 0$ and one where $ks \approx \infty$.

As an intermediate problem, we consider the case in which c solves (4.12a) and (4.12b), on a fixed perforated domain, with zero interior boundary condi-

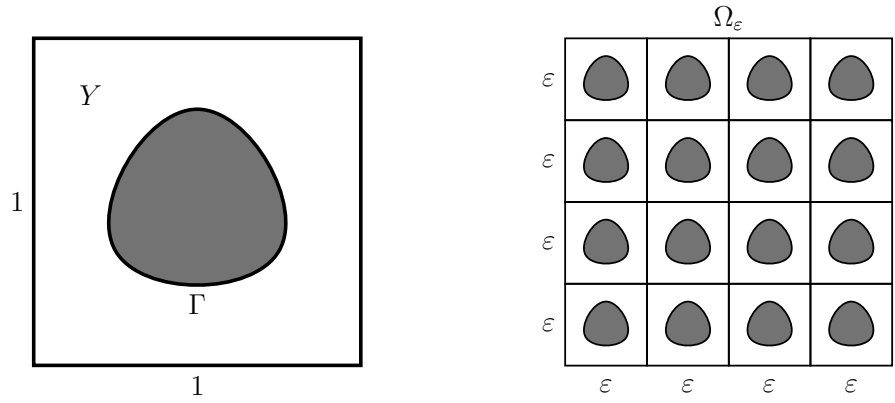

Figure 4.2: Geometry of the unit cell (left) and the perforated domain (rigth). We have indicated the boundary $\Gamma = Y \cap \partial A$ in the unit periodic cell on the left.

tions:

$$c_t = D\Delta c \qquad \text{for } x \in \Omega_\varepsilon,\ t > 0 \tag{4.13a}$$
$$c = 0 \qquad \text{for } t > 0 \text{ and } x \in \Gamma_\varepsilon \tag{4.13b}$$
$$c = c_b \qquad \text{for } t > 0 \text{ and } x \in \partial\Omega_\varepsilon \setminus \Gamma_\varepsilon \tag{4.13c}$$
$$c = c_i \qquad \text{for } t = 0 \text{ and } x \in \Omega_\varepsilon. \tag{4.13d}$$

Here Ω_ε is a perforated version of Ω, constructed in the following way. Let $A \subset \mathbb{R}^n$ be a 1-periodic subset of $\mathbb{R}^n$ (i.e. $A + e_i = A$ for all unit base vectors e_i), and set $A_\varepsilon = \varepsilon A$. We write Y for the unit periodic cell of A, $Y = [0,1]^n \cap A$. Define Ω_ε by

$$\Omega_\varepsilon = \Omega \cap A_\varepsilon.$$

The internal boundary Γ_ε is given by $\Gamma_\varepsilon = \Omega \cap \partial A_\varepsilon$, see also Figure 4.2.

In the limit $\varepsilon \to 0$, the ratio of the area of Γ_ε to the volume Ω_ε is unbounded, and therefore the solution of (4.13) converges pointwise to zero as $\varepsilon \to 0$. We take this fast decay of the solution into account by posing the following *Ansatz* of the solution c^ε:

$$c^\varepsilon(x,t) = e^{-D\lambda t/\varepsilon^2} c_0(x,t) w\Big(\frac{x}{\varepsilon}\Big),$$

where λ is the first eigenvalue of $-\Delta$ on A with homogeneous Dirichlet boundary conditions. Here c_0 is defined on $\Omega \times [0,\infty)$ and w on Y. On substitution into (4.13a) we find, writing y for x/ε,

$$\begin{aligned} 0 = {} & \varepsilon^{-2}\, c_0(x,t)\big[\, D\Delta w(y) + D\lambda w(y) \,\big] \\ & + \varepsilon^{-1}\, 2D\nabla c_0(x,t) \cdot \nabla w(y) \\ & + \varepsilon^{0}\, w(y)\big[\, D\Delta c_0(x,t) - c_{0t}(x,t) \,\big] \end{aligned} \tag{4.14}$$

By the choice of λ, the equation at level ε^{-2} forces w to be a multiple of the first eigenfunction. This function w is therefore also the first eigenfunction of $-\Delta$ on Y with the following boundary conditions:

$$\begin{aligned}&\text{periodic conditions on } \partial Y \cap \partial[0,1]^n;\\ &\text{homogeneous Dirichlet conditions on } \partial Y \setminus \partial[0,1]^n.\end{aligned}$$

Since we can multiply w by a constant, and divide c_0 by the same constant without changing c, we choose to normalize w by assuming

$$\int_Y w(y)\,dy = 1.$$

Integrating (4.14) over Y and using the periodicity of w, the integral at level ε^{-1} vanishes, and we are left with

$$c_{0t} = D\Delta c_0 \qquad \text{for } x \in \Omega,\ t > 0.$$

The function c^ε is therefore approximated by the solution of the equation

$$c_t = D\Delta c - \frac{D\lambda}{\varepsilon^2} c \qquad \text{for } x \in \Omega,\ t > 0. \tag{4.15}$$

To make the connection back to the Stefan problem, we note that the parameter λ in (4.15) is determined by solving an eigenvalue problem on the perforated unit cell Y. We now need to make an assumption on how we may deduce the microscopic geometry from a given macroscopic scavenger concentration s—for instance, we could assume that in the unit cell the scavenger is contained in a sphere of concentration $\overline{s}$; the macroscopic concentration then determines the radius of this sphere (see also below).

Under such an assumption, the parameter λ is a function of the macroscopic scavenger concentration s, and the macroscopic oxygen concentration c satisfies the equation

$$c_t = D\Delta c - \frac{D\lambda(s)}{\varepsilon^2} c.$$

By mass conservation—the difference $c-s$ is conserved locally in (4.10a), therefore the same is true for the homogenized concentration—the equation for s is

$$s_t = -\frac{D\lambda(s)}{\varepsilon^2} c.$$

By doing this we are treating the geometry as quasi-static in the c-equation, *i.e.* we assume that the geometry does not change on the time scale of the c-equation. This depends on the concentration of s, as can be seen in (4.12c); it means that the ratio C/S is small, where C and S are typical scales of the initial concentrations c_i and s_i.

Finally, let us analyse the asymptotic behaviour of the eigenvalue λ for small scavenger concentrations s. We will approximate the eigenvalue problem for

the Laplacian on a unit cell $Y = [0,1]^n \cap A$ by one on a unit ball with a much smaller ball $B_{r_0}(0)$. inside. Furthermore, we replace the periodic boundary conditions by Neumann boundary conditions. It is our firm believe that these approximations do not influence the asymptotic result for small s. Since the first eigenfunction will be symmetric, we arrive at the problem

$$\begin{aligned} c_{rr} + \tfrac{2}{r} c_r + \lambda c = 0 \qquad & \text{for } r_0 < r < 1 \\ c(r_0) = 0 & \\ c_r(1) = 0 & \end{aligned}$$

The general solution of the differential equation is

$$c(r) = C_1 \frac{\sin(\sqrt{\lambda} r)}{r} + C_2 \frac{\cos(\sqrt{\lambda} r)}{r}.$$

Applying the boundary conditions leads, after some calculations, to $\lambda \sim 3r_0$ as $r_0 \to 0$. In terms of the scavenger concentration s this translates to $\lambda(s) \sim Cs^{1/3}$ for small s.

When we compare this to the analogous two-dimensional problem, representing very elongated droplets, we find $\lambda(s) \sim C|\ln s|^{-1}$ for small s. This suggests that small elongated droplets lead to higher values of λ and thus a more effective scavenger in this limit problem.

Summary

If we assume that the parameter $\alpha = D/\varepsilon^2 kS$ is large, then we find in the limit $\varepsilon \to 0$ the homogenized equations

$$\begin{aligned} c_t &= D\Delta c - kcs \qquad && \text{for } x \in \Omega,\ t > 0 \\ s_t &= -kcs && \text{for } x \in \Omega,\ t > 0. \end{aligned}$$

On the other hand, if α is small, then we find as limit equations

$$c_t = D\Delta c - \frac{D\lambda(s)}{\varepsilon^2} c \qquad \text{for } x \in \Omega,\ t > 0 \tag{4.16a}$$

$$s_t = -\frac{D\lambda(s)}{\varepsilon^2} c \qquad \text{for } x \in \Omega,\ t > 0 \tag{4.16b}$$

where λ is determined from s as described above, and the asymptotic behaviour for small concentrations is $\lambda \sim Cs^{1/3}$ and $\lambda \sim C|\ln s|^{-1}$ for small spherical and thin elongated droplets, respectively.

There is a paradox in this: the parameter α itself depends on ε. For the diffusion-dominated case this does not matter, since the limit $\varepsilon \to 0$ is consistent with the assumption that α is small. In the reaction-dominated case, however, the limit $\varepsilon \to 0$ entails large values of α. The statement above should therefore be understood as a description of intermediate asymptotics: in the parameter regime in which both α and ε are small, the problem (4.16) is expected to approximate the problem (4.10). For any fixed k and D, in the limit $\varepsilon \to 0$ the system will *eventually* be diffusion-dominated.

4.4 Behavior of the penetration time in one dimension

Although the reaction-diffusion scheme described by equations (4.2a) and (4.2b) is hard to analyze (mainly because of the nonlinearities and the absence of nonzero equilibrium points), it is possible to do so under some physical assumptions, that are explained below. These assumptions were discussed with the problem owners and seemed valid. In section 4.3 the effects of the shape of the droplets is discussed. In this section we consider the one-dimensional case where the packaging material consists of two layers of foil (without scavenger material) and one layer of pure scavenger material (Figure 4.3).

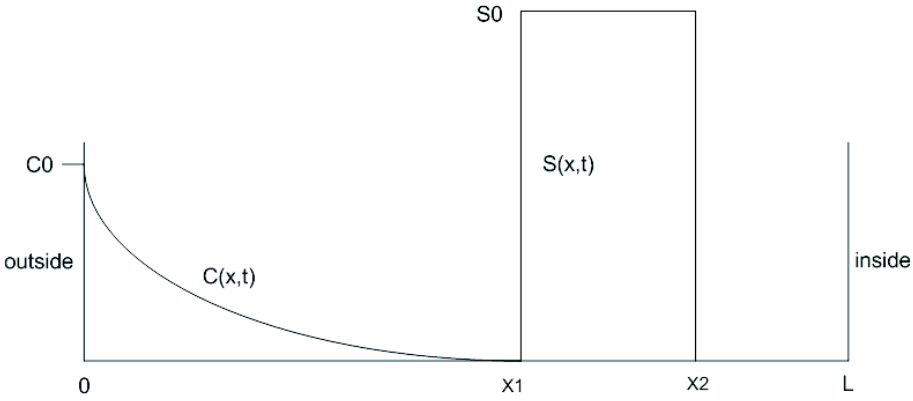

Figure 4.3: One-dimensional cross-section of packaging material

In this figure, C_0 denotes the oxygen concentration on the outside, S_0 the initial scavenger concentration, x_1 and x_2 the initial boundaries of the scavenger layer, $c(x,t)$ the oxygen profile within the packaging material, and L the thickness of the material.
The objective is now to express the time that the oxygen needs to penetrate the material (penetration time) as a function of the physical coefficients. We consider three time intervals; t_1, t_2 and t_3, that denote the penetration times for layers 1,2 and 3 respectively.

Penetration time for a layer of foil

The typical penetration time for the first layer of foil is expressed in terms of the Fourier number for mass transport

$$\mathrm{Fo} = \frac{D\tau}{d^2}, \tag{4.17}$$

where D is the mass diffusion coefficient, and τ the penetration time for a layer with thickness d; see for example [3] or any standard book on physical transport phenomena. This number relates a specifically chosen 'critical' flux

after time τ, to the penetration time for the same flux with different values for parameter d. For some critical flux, Fo can be measured experimentally. Theoretically, we would like to know the time before *some* oxygen reaches the scavenger boundary, but since the process is modelled by a diffusion equation, the oxygen concentration is nonzero over the whole layer of foil instantly. Hence the assumption of a critical flux to mark the penetration time. From equation (4.17) it follows that the penetration time for the first layer of foil is

$$t_1 = \frac{\mathrm{Fo} x_1^2}{D}. \tag{4.18}$$

Penetration time for a layer of scavenger material

When oxygen reaches x_1, the scavenger reacts with the oxygen and vanishes. The left side of the layer of scavenger will start reacting away and leave a layer of pure foil. This means that boundary $x_2(t)$ will move to the right. In order to compute the penetration time for a layer of scavenger material, we make two extra assumptions. The first assumption is that S_0 is 'large enough', so that once the oxygen reaches x_1, $c(x,t)$ settles quickly to an equilibrium profile, while $x_2(t)$ moves only a little. The second assumption is that the scavenger reacts very quickly with oxygen, so that at $x_2(t)$ the oxygen concentration is approximately zero. (The second assumption holds true if the Thiele modulus $\mathrm{Th} = d_s\sqrt{\frac{\kappa}{D}}$ is large. This dimensionless quantity indicates the dominance of chemical reaction rate over diffusive mass transfer rate). These assumptions lead us to the following. Once a critical amount of oxygen reaches x_1, $c(x,t)$ settles quickly into its equilibrium profile, which is a time-varying linear function with boundary conditions $c(0) = C_0$ and $c(x_2(t)) = 0$. According to Fick's law [3] the oxygen flux at $x_2(t)$ is

$$-D\frac{dc(x_2(t))}{dx_2(t)} = \frac{DC_0}{x_2(t)}. \tag{4.19}$$

The amount of scavenger that disappears after reaction is

$$S_0\frac{dx_2(t)}{dt}. \tag{4.20}$$

Since an amount of β particles of oxygen react with α particles of scavenger, the mass balance reads

$$\beta\frac{DC_0}{x_2(t)} = \alpha S_0\frac{dx_2(t)}{dt}, \tag{4.21}$$

with initial condition $x(0) = x_1$. The solution to equation (4.21) is

$$x_2(t) = \sqrt{\frac{2\beta C_0 Dt}{\alpha S_0} + x_1^2}. \tag{4.22}$$

The penetration time t_2 is obtained by solving

$$x_2 = \sqrt{\frac{2\beta C_0 Dt_2}{\alpha S_0} + x_1^2}, \tag{4.23}$$

which gives

$$t_2 = \frac{\alpha S_0(x_1^2 - x_1^2)}{2\beta D C_0} \tag{4.24}$$

$$= \frac{\alpha S_0 d_s(x_1 + x_2)}{2\beta D C_0}, \tag{4.25}$$

with d_s the thickness of the scavenger layer.

Total penetration time

The penetration time for the third layer, t_3, is computed similarly to t_1

$$t_3 = \frac{\mathrm{Fo}(L - x_2)^2}{D} \tag{4.26}$$

$$= \frac{\mathrm{Fo}(d_s + x_1)^2}{D}. \tag{4.27}$$

The total penetration time is now

$$t_{total} = \frac{\mathrm{Fo}x_1^2}{D} + \frac{\alpha S_0 d_s(x_1 + x_2)}{2\beta D C_0} + \frac{\mathrm{Fo}(d_s + x_1)^2}{D}. \tag{4.28}$$

Equation (4.28) is of the form

$$a_1 x_1 + a_2 S_0 d_s^2 + a_3 S_0 x_1 d_s + a_4 d_s, \tag{4.29}$$

with a_i positive. The total penetration time increases with d_s quadratically, and with x_1 and S_0 linearly.
For further investigation, we would like to pose the idea of relating the penetration time of the scavenger layer to a dimensionless number, similar to the Fourier number. As was mentioned before, the assumptions are discussed with DSM, but of course need scientific validation.

4.5 Solution procedure for the stationary problem via conformal mapping

To test the effect of changing the shape and form of the scavenger droplets inside the foil, a simplified model is assumed, where the foil is modeled as an infinite strip with one block of scavenger in the middle of height $2h$ and width $2L$ (see figure 4.4). The thickness of the strip is rescaled to 2. Obviously we are interested in those values of h and L for which we have the smallest flux of oxygen reaching the food.

The stationary problem

The system of equations (4.2a) and (4.2b) is difficult to solve analytically and does not have any non-trivial stationary solutions. However, a stationary solution can be found if we look at a slightly different problem. We consider

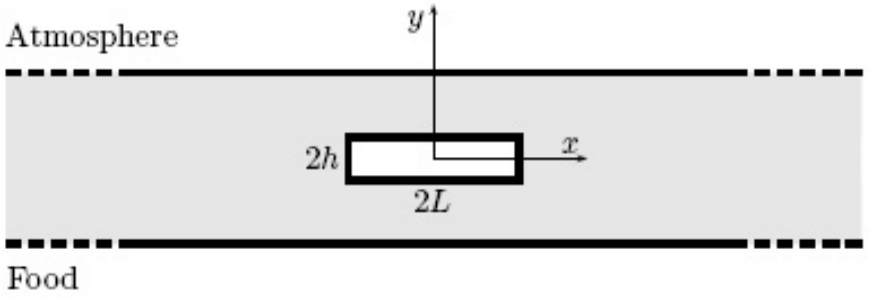

Figure 4.4: Foil modeled as an infinite strip with a rectangular piece of scavenger.

the case of a high reaction speed, so that any oxygen reaching the scavenger boundary will react away immediately. Furthermore the block is assumed to be saturated, so that there is an unlimited supply of scavenger. As a result the oxygen concentration at the boundary of the block will always be equal to zero and the scavenger concentration will be constant in time. Outside the block the oxygen concentration can be described by the diffusion equation, of which the stationary solutions satisfy Laplace's equation. Finally we also assume that the oxygen reacts away with the food immediately so that at the side of the food we also have $c = 0$. At the other side of the foil the concentration of oxygen can be assumed constant and is scaled in such a way that $c = 1$.

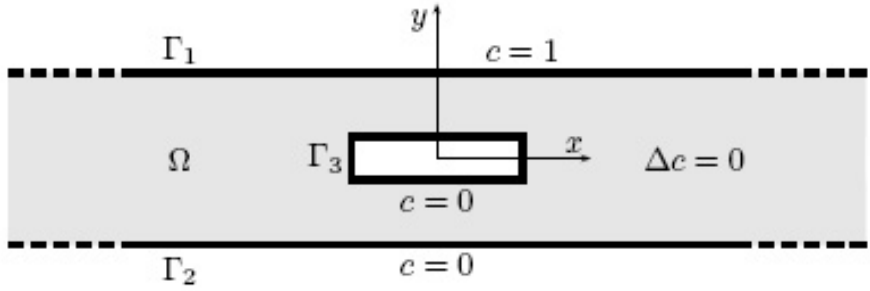

Figure 4.5: Boundary value problem on an infinite strip excluding a rectangular piece of scavenger.

Now let Ω be the two-dimensional domain that consists of an infinite strip excluding a rectangle of length $2L$ and width $2h$:

$$\Omega := \{(x, y) \in \mathbb{R}^2 : -1 < y < 1\} \setminus ([-L, L] \times [-h, h]),$$

and let $\Gamma = \Gamma_1 \cup \Gamma_2 \cup \Gamma_3$ be the boundary of Ω, where Γ_1 is the boundary with the environment, Γ_2 is the boundary with the food and Γ_3 the boundary of the

block, as indicated in figure 4.5. On this geometry we want to solve

$$\Delta c = 0, \qquad (x, y) \in \Omega, \tag{4.30a}$$

subject to

$$c = 1, \qquad (x, y) \in \Gamma_1, \tag{4.30b}$$
$$c = 0, \qquad (x, y) \in \Gamma_2 \cup \Gamma_3. \tag{4.30c}$$

This problem can describe the oxygen concentration for small time, when none of the scavenger has reacted away completely. Moreover data provided by DSM indicated that initially the amount of permeated oxygen did not change much in time, suggesting stationary behaviour.

The boundary value problem in (4.30) still seems difficult to solve because of the complexity of the domain. However, using the theory of conformal mappings [6], solving Laplace's equation can be reduced to solving a potential problem on an easier domain in the complex plane.

Solution using conformal mappings

We identify the geometry in figure 4.5 with the complex plane. Because of symmetry we can restrict ourselves to that part of Ω where x is positive, which will be denoted by Ω_1 (see figure 4.6):

$$\Omega_1 := \{z \in \mathbb{C} : (\operatorname{Re} z, \operatorname{Im} z) \in \Omega \wedge \operatorname{Re} z > 0\}.$$

Consequently an extra Neumann boundary condition $\partial c/\partial n = 0$ arises at $x = 0$, where n is the outward normal vector. We introduce the points A, B, C, D, E, F and G by $A = \mathrm{i}$, $B = h\mathrm{i}$, $C = L + h\mathrm{i}$, $D = L - h\mathrm{i}$, $E = -h\mathrm{i}$, $F = -\mathrm{i}$ and $G = \infty \pm \mathrm{i}$, as indicated in figure 4.6.

A map $f : \Omega_1 \to \Omega_2$ is called a conformal mapping if $f(z)$ is analytical and one-to-one in Ω_2. Furthermore $f^{-1} : \Omega_2 \to \Omega_1$ exists and is also a conformal mapping. Throughout this section we will implicitly use the following two theorems [6]:

Theorem 4.5.1. *Riemann mapping theorem:*
For any two simply connected open subsets Ω_z, Ω_w of the complex plane $\mathbb{C}$ that are not all of $\mathbb{C}$ and for given $z_0 \in \Omega_z$, $w_0 \in \Omega_w$, $\alpha \in \mathbb{R}$, there exists a unique conformal map $f : \Omega_z \to \Omega_w$ such that $f(z_0) = w_0$ and $\arg(f'(z_0)) = \alpha$.

Theorem 4.5.2. *Carathéodory's theorem:*
For any pair of simply connected open sets Ω_z and Ω_w bounded by Jordan curves Γ_z and Γ_w, a conformal map $f : \Omega_z \to \Omega_w$ can be extended continuously to the boundary, giving a homeomorphism $F : \Gamma_z \to \Gamma_w$. Furthermore, if z follows the boundary Γ_z in a positive way, then also $w = f(z)$ will follow the boundary in a positive way.

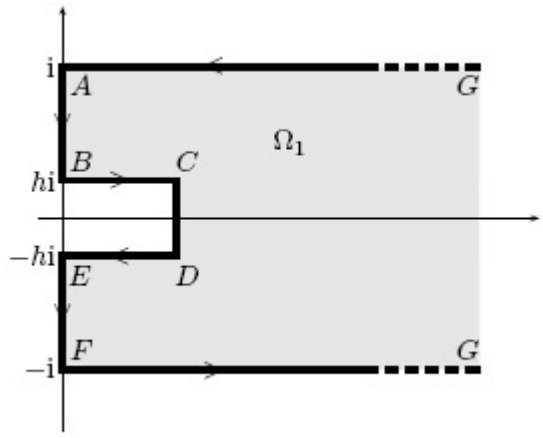

Figure 4.6: Right part of the foil identified with a subset of the complex plane.

Note that in theorem 4.5.1 the conformal map f is uniquely determined by the three conditions: $\mathrm{Re}(f(z_0)) = \mathrm{Re}(w_0)$, $\mathrm{Im}(f(z_0)) = \mathrm{Im}(w_0)$ and $\arg(f'(z_0)) = \alpha$.

We would like to use conformal mappings to map Ω_1 to the upper half plane, on which a solution is easier to compute. By the Schwarz-Christoffel formula [6] we can construct a conformal mapping f_1 from the upper half plane $\Omega_2 := \{w \in \mathbb{C} : \mathrm{Im}\, w > 0\}$ to the unbounded polygon Ω_1 (see figure 4.7),

$$f_1(w) = C_1 \int_0^w \frac{\sqrt{\tilde{w} - w_C}\sqrt{\tilde{w} - w_D}}{\sqrt{\tilde{w} - w_A}\sqrt{\tilde{w} - w_F}\sqrt{\tilde{w} - w_B}\sqrt{\tilde{w} - w_E}}\, \mathrm{d}\tilde{w} + D_1,$$

where $C_1, D_1 \in \mathbb{C}$ are yet to be determined. The path of integration should be chosen in the upper half plane and f_1 is such that the points $w_A, w_B, \ldots, w_G$ are mapped onto the points $A, B, \ldots G$ in Ω_1. We have the freedom to choose three of the real points $w_A, w_B, \ldots, w_G$. This will fix the remaining points. Let us take $w_G = \infty$, $w_B = -1$ and $w_E = 1$. Because of symmetry we have $w_D = -w_C$ and $w_F = -w_A$. Since $f_1(0) = L$, again by symmetry, we have

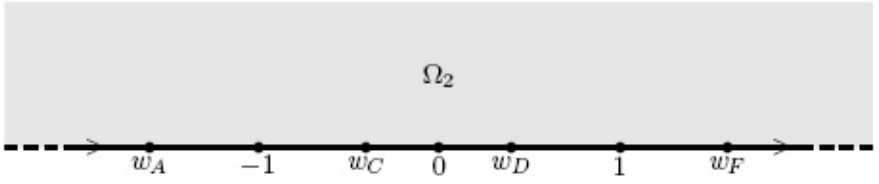

Figure 4.7: f_1^{-1} will map the unbounded polygon Ω_1 onto the complex upper half plane Ω_2.

$D_1 = L$. This leads to

$$f_1(w) = C_1 \int_0^w \frac{\sqrt{\tilde{w} - w_C}\sqrt{\tilde{w} + w_C}}{\sqrt{\tilde{w} - w_A}\sqrt{\tilde{w} + w_A}\sqrt{\tilde{w} + 1}\sqrt{\tilde{w} - 1}} \, \mathrm{d}\tilde{w} + L. \tag{4.31}$$

For C_1 and the negative numbers w_A and w_C we know that $w_A < -1$ and $-1 < w_C < 0$ and they can be determined from the following system of three equations with three unknowns:

$$f_1(w_A) = \mathrm{i}, \tag{4.32a}$$
$$f_1(-1) = h\mathrm{i}, \tag{4.32b}$$
$$f_1(w_C) = L + h\mathrm{i}. \tag{4.32c}$$

The inverse function f_1^{-1} is also conformal and will map Ω_1 onto Ω_2.

If there were only Dirichlet boundary conditions then a solution would be easy to find. The real part and the imaginary part of an analytic function $x + \mathrm{i}y \mapsto \phi(x + \mathrm{i}y)$ can be regarded as an harmonic function in x and y. The function $\arg(w - w_A)$ is the imaginary part of the analytic function $\ln(w - w_A)$ and will therefore be harmonic in the complex upper half plane. Furthermore it also satisfies the conditions $c = 1$ on the segment GA, and $c = 0$ on BE. However, the Neumann boundary condition $\partial c/\partial n = 0$ is not satisfied on AB and EF. Therefore we would like to map Ω_2 onto a domain where we can satisfy all boundary conditions.

Knowing w_A, w_C and C_1, we can construct another Schwarz-Christoffel mapping $f_2 : \Omega_2 \to \Omega_3$ where Ω_3 has the geometry that is drawn in figure 4.8. The mapping will be of the form

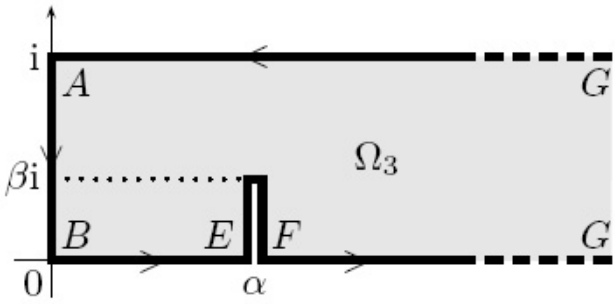

Figure 4.8: Geometry of Ω_3.

$$f_2(w) = C_2 \int_0^w \frac{\tilde{w} - \gamma}{\sqrt{\tilde{w} - w_A}\sqrt{\tilde{w} + 1}\sqrt{\tilde{w} - 1}\sqrt{\tilde{w} + w_A}} \, \mathrm{d}\tilde{w} + D_2, \tag{4.33}$$

where γ is some real number. Again the path of integration is in the upper half plane. This mapping maps Ω_2 to a set that has boundary angles $\frac{\pi}{2}$ at the points A, B, E and F. There exists a $\gamma \in \mathbb{R}$, such that E and F coincide and

the boundary of Ω_3 makes an angle of 2π at $\alpha+\beta\mathrm{i} := f_2(\gamma)$, as shown in figure 4.8, and

$$\Omega_3 = \{z \in \mathbb{C} : \mathrm{Re}(z) > 0,\ 0 < \mathrm{Im}(z) < 1\} \backslash \{z \in \mathbb{C} : \mathrm{Re}(z) = \alpha,\ 0 < \mathrm{Im}(z) < \beta\}.$$

The lengths of the segments of the boundary, however, are not fixed yet. We determine C_2, D_2 and γ from the three equations:

$$f_2(-1) = 0, \tag{4.34a}$$
$$f_2(w_A) = \mathrm{i}, \tag{4.34b}$$
$$f_2(1) = f_2(-w_A). \tag{4.34c}$$

Now, B will be located in the origin in Ω_3, A will be at i and the points E and F coincide in Ω_3, like in figure 4.8. Note that automatically $f_2(\infty) = \infty$.

The real part and the imaginary part of an analytic function $x + \mathrm{i}y \mapsto \phi(x + \mathrm{i}y)$ can be regarded as an harmonic function in x and y. The imaginary part $\tilde{c}$ of the analytic function $\phi(z) = z$ is equal to $\mathrm{Im}(z) = y$ and satisfies the conditions $\tilde{c} = 1$ on the segment GA, $\partial\tilde{c}/\partial n = 0$ on AB, $\tilde{c} = 0$ on BE, $\partial\tilde{c}/\partial n = 0$ on EF and $\tilde{c} = 0$ on FG. Therefore $\tilde{c}(x, y) = y$ solves the boundary value problem on $I(\Omega_3)$, where $I : \mathbb{C} \to \mathbb{R}^2$ is given by

$$I(x + \mathrm{i}y) = (x, y).$$

We have a conformal mapping $f : \Omega_1 \to \Omega_3$, namely

$$f = f_2 \circ f_1^{-1}.$$

Compositions of harmonic functions with conformal mappings are again harmonic functions. The solution $c : \Omega \to \mathbb{R}$ of the original problem is therefore given by

$$c = \tilde{c} \circ I \circ f \circ I^{-1} = \mathrm{Im} \circ f \circ I^{-1}.$$

In other words

$$c(x, y) = \mathrm{Im}\left(f_2(f_1^{-1}(x + \mathrm{i}y))\right). \tag{4.35}$$

Results

Using conformal mappings we have reduced solving boundary value problem (4.30) to solving the two systems of equations (4.32) and (4.34). These can be solved numerically and possibly even analytically. Once the unknown constants are found, equation (4.35) will yield the oxygen concentration and thus the permeating oxygen can be calculated.

To test which scavenger configuration is better, we need some kind of measure for the oxygen exposure. Of course a configuration is better if the total flux of oxygen through Γ_3 (see figure 4.5) becomes smaller. Thus we would like to minimize:

$$\int_{-\infty}^{\infty} \frac{\partial c}{\partial \mathbf{n}}(x, -1)\ \mathrm{d}x = 2\int_{0}^{\infty} \frac{\partial c}{\partial \mathbf{n}}(x, -1)\ \mathrm{d}x.$$

However, this integral could be divergent. For large x the oxygen flux will not be affected by the presence of the block, therefore a suitable alternative could be the following: for $s > 0$ introduce the average flux F_s defined as

$$F_s(L,h) := \frac{1}{s}\int_0^s \frac{\partial c}{\partial \mathbf{n}}(x,-1;L,h)\ \mathrm{d}x.$$

Now for a given area C and fixed s large enough we can compare different configurations with $L * h = C$ by computing for which configuration F_s is smallest.

The previous analysis can also be performed for a bounded strip rather than an infinite strip. The advantage of such a model is that periodic boundary conditions can be assumed on both ends and thus a whole series of scavenger blocks can be modelled. However, the Schwarz-Christoffel formula f_1 in (4.31) would get an additional constant that has to be determined. This would complicate the analysis slightly because now we get an extra Neumann boundary condition and four equations with four unknowns have to be solved rather than three equations with three unknowns. This approach is more realistic since the foil contains more than one scavenger droplet, whereas only minor extra complications arise.

Finally, we could also consider the two limiting cases $(L,h) \to (0,C)$ and $(L,h) \to (C,0)$. These two cases show the extremes of stretching in the horizontal and vertical direction and could already give an indication which kind of stretching is better. Moreover, it simplifies the analysis. In these two cases only two equations have to be solved to find Ω_2. Also this simplification might allow us to solve the integral expression for f_1 explicitly, so that the system (4.32) transforms into a system of two algebraic equations. Calculating f_2 remains as difficult as it was.

4.6 One-dimensional numerical simulation

We have done simulations in one and two space dimensions. The one-dimensional experiments are described in this section, the two-dimensional simulations in section 4.7. Full numerical simulations of the three-dimensional model turned out not be feasible in the one week period of the Study Group. Even with more time available it is not certain that a three-dimensional model can be computed with accuracy within a reasonable time period.

In order to find numerical approximations we have to make some assumptions and set some boundary and initial conditions. For both the one- and two-dimensional simulations we have taken the following conditions.

- The time domain has been scaled to $[0,1]$. The space domain has been scaled to $\Omega = [0,1]$ for the one-dimensional simulations and $\Omega = [0,1] \times [0,1]$ for the two-dimensional simulations (see section 4.7).
- $c(x,0) = 0$, at the start there is no oxygen in the material

- $c(0,t) = 0$, $c(1,t) = c_a$. At the food boundary of the foil, i.e. $x = 0$, the oxygen concentration is zero; at the other boundary the concentration of oxygen is constant.
- $s(x,0) = \phi(x)$, the initial concentration of scavenger material is a prescribed function of the position.

The initial scavenger concentration should describe the scavenger material that is present in the droplets in the foil. These droplets are spherical when the foil is created. However the foil can also be stretched in the fabrication process. This stretching can occur in either one or two directions leading to cigar or pancake shaped droplets, respectively. In the numerical simulations we have used rectangular bump functions for the initial scavenger concentrations. This choice was done for convenience but other initial concentrations (such as perfect spheres, cigars or pancakes) can also be analyzed numerically. An argument for our choice of rectangular bump functions is that the partial differential equation used to model the process is a diffusion equation with a reaction term. The diffusion term has the property that all solutions will be smooth (even for non-smooth initial conditions).

Topological effects

We expect that the two- and three-dimensional models will be quite different from the one-dimensional model for topological reasons. In figure 4.9 we have a schematic picture of the foil for the two-dimensional model. The scavenger droplets are indicated as black spots. The oxygen particles can go through the foil in various paths. We have drawn three different type of paths in the figure. The dotted path represents an oxygen particle that enters the foil, but is absorbed by a scavenger particle. The dashed path is the path of a particle that enters the foil, passes through a droplet but is not absorbed. Finally the oxygen particle reaches the food boundary. In solid black there are two paths where the oxygen particle passed through the foil without encountering any scavenger material. The black paths cannot occur in the one-dimensional model. There every oxygen particle that passes through the foil will have to pass through one or more droplets (assuming that there is at least one droplet).

One-dimensional simulations

The one-dimensional simulations are important to get a feeling for the possible three-dimensional results. For various initial configurations of scavenger material a numerical solution was calculated using Mathematica. The function `NDSolve` has been used to find a numerical approximation to the partial differential equation.

The initial scavenger configurations that have been analyzed are

- A homogeneous scavenger concentration.
- Bump functions with a various number of bumps.

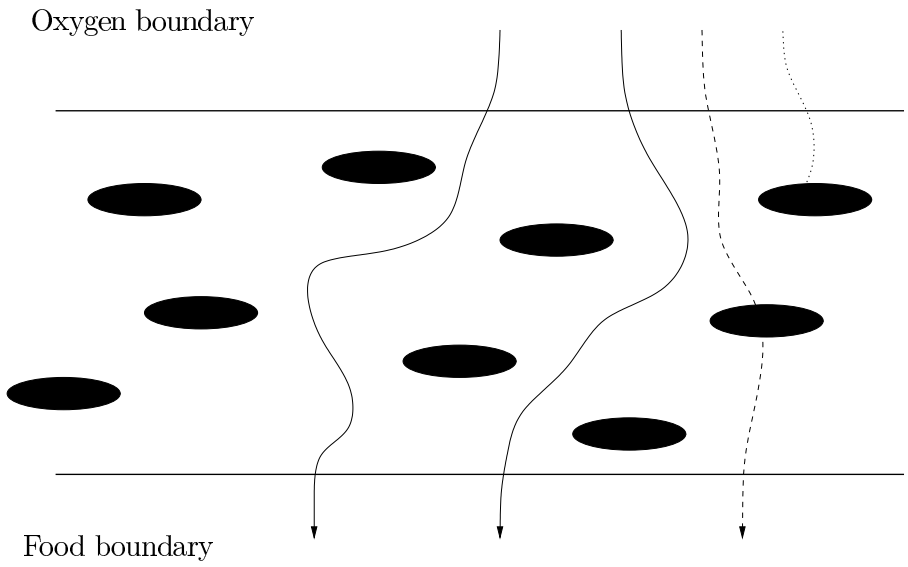

Figure 4.9: Oxygen paths in the foil

During the simulations we found out that the results depend very sensitively on the values of the parameters. We will give a few examples that illustrate the various phenomena that can occur. In the simulations described below we have taken $\alpha = \beta = 1$, $D = 1$, $\kappa_c = 50, \kappa_s = 1$ and $c_a = 1$.

Four bump scavenger configuration

In figure 4.10 we have plotted the initial scavenger concentration for a four-bump scavenger concentration. Given the initial conditions described above we can find a numerical solution to the system of partial differential equations (4.2a)-(4.2b) for this particular initial scavenger concentration. In figure 4.11 we have plotted the scavenger configuration as a function of time and position. We can see that one by one the droplets of scavenger material are shrinking because of absorption of oxygen.

High reaction rate limit

In the limit of a very high reaction rate the scavenger material reacts almost instantly with the oxygen. In this situation no oxygen can penetrate the foil until all the scavenger material has been absorbed. The absorption rate of the scavenger material is determined by the distance of the scavenger material to the oxygen boundary. Here we can say the the best distribution of scavenger material is placing all the scavenger material close to the food boundary.

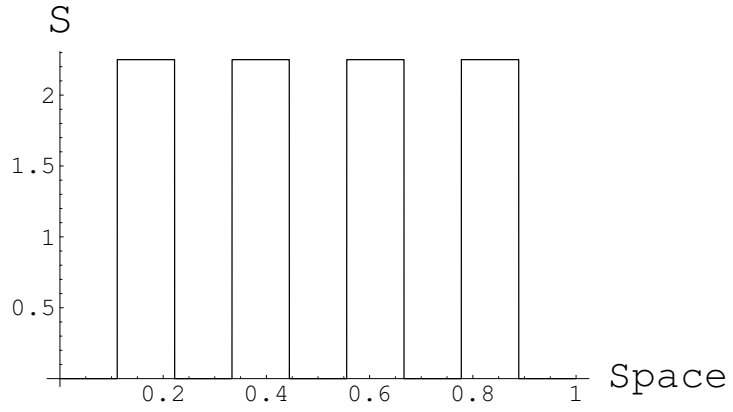

Figure 4.10: Initial scavenger concentrations in the four-bump configuration

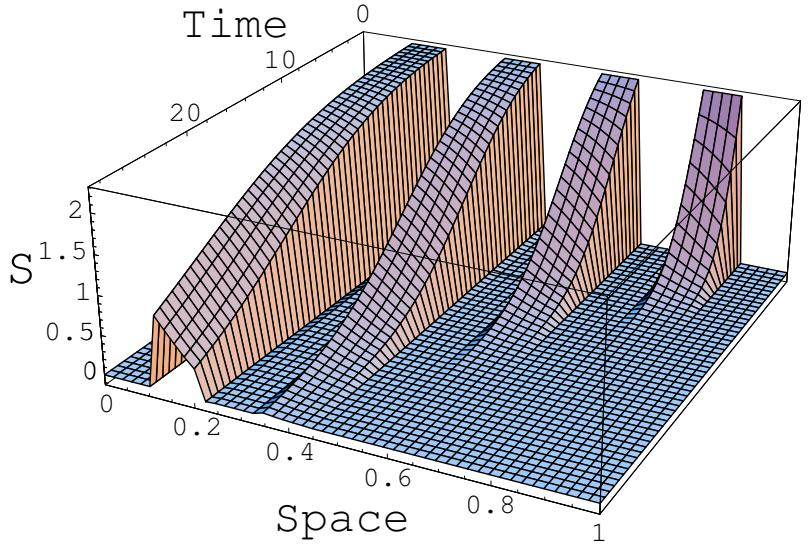

Figure 4.11: Scavenger concentrations for the four-bump configuration

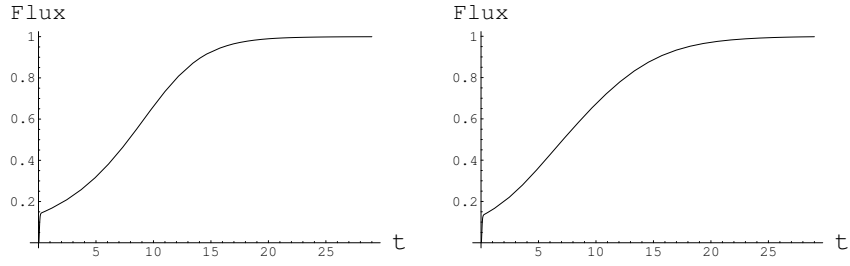

(a) 1-bump (b) 2-bump

Figure 4.12: Flux for various scavenger configuration

Time scales

We compare a one bump scavenger concentration with a two bump scavenger concentration. The flux of oxygen has been plotted for both configurations and also the difference in flux. This flux (and the integral of the flux over time) is a measure for the amount of oxygen that reaches the food and hence a measure of how good the foil is.

In figure 4.12 the flux for the one-bump configuration was plotted. In the plot for the flux we can see 3 time domains:

Oxygen spreading through the foil This happens very quickly and is a consequence of the diffusion equation used to model the process. In the plot above the timescale is roughly 0.1 time units.

Reaction The scavenger material reacts with the oxygen that diffuses through the foil. During this period the amount of scavenger material decreases and as a result the flux and concentration of oxygen in the foil increases.

Final state For this simulation the final state is reached after roughly 20 time units. All the scavenger material has reacted with the oxygen and the numerical solution approaches the exact solution in the case of no scavenger material.

The flux for the one-bump and two-bump configurations looks very similar. However if we plot the difference of flux we get an interesting picture. In figure 4.13 the difference is shown. We can see that at the start, up to $t \approx 1.5$, the flux for the one-bump configuration is higher. Hence the foil with a two-bump configuration performs better than the foil with the one-bump configuration. From $t \approx 1.5$ to $t \approx 10.6$ the one-bump foil performs better. For larger values of t the two-bump performs better. In the limit the scavenger material in both foils has reacted away and the flux in both foils becomes identical. If we integrate the flux we get the total amount of oxygen that has passed through the foil. The integral of the flux difference from figure 4.13 is plotted in figure 4.14. Here we see that also for the total amount of oxygen the

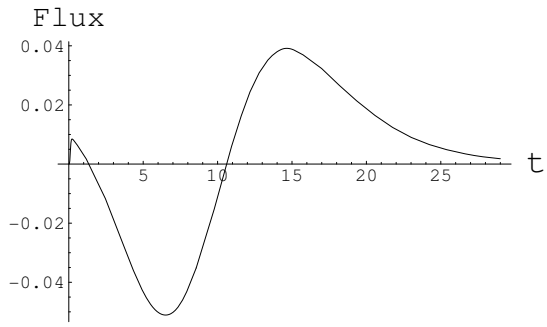

Figure 4.13: Flux difference between one-bump and two-bump scavenger configuration

one-bump configuration performs better for small time, but worse for t between 2.5 and 20.5 and again better for t larger then 20.5.

The results may seem surprising but can give an intuitive explanation as follows. Scavenger material is more effective if it is closer to the oxygen boundary. From the one-bump and two-bump configurations, the bump close to the oxygen boundary in the two-bump configuration is closest to the oxygen boundary. Therefore for small t this bump will make the two-bump configuration perform better. However, since this bump is close to the oxygen boundary it also reacts faster with the oxygen than the other bumps. After some time this bump will have been reduced by reaction and the bump in the one-bump configuration becomes dominant; this makes the one-bump configuration perform better. If also this bump is reacted away for the most part the last bump, the bump close to the food boundary in the two-bump configuration, dominates and makes the two-bump foil again perform better. The explanation above is only an intuitive one: for other configurations only a numerical calculation can give the flux and total amount of oxygen as a function of time.

4.7 Two-dimensional numerical simulation

two-dimensional numerical simulations

Simulations in two-dimensions were made in order to investigate the difference between shapes of scavenger droplets and oxygen flux through the film. We model the film as an infinitely long strip consisting of one layer of rectangular cells (see Figure 4.15). Each cell has a rectangular scavenger particle in the center and the particle occupies 10% of the cell. At the outer side of the film there is normal air and the oxygen concentration is c_a; at the inner side the oxygen concentration is 0 (oxygen immediately reacts with the food). Initially there is no oxygen in the film.

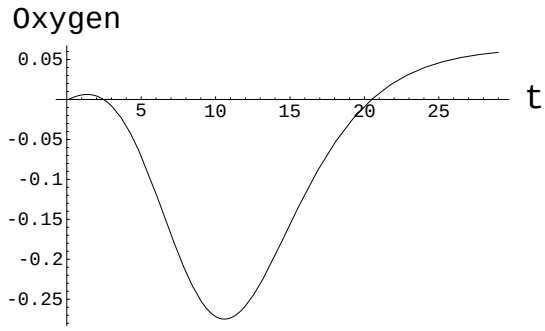

Figure 4.14: Difference between the total amount of oxygen passed between one-bump and two-bump scavenger configuration

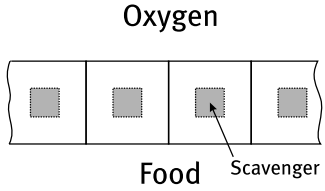

Figure 4.15: Two-dimensional model of the film with scavenger droplets. The film consists of one layer of rectangular elements. Each element has one scavenger particle in the center.

We proceed with a cell of length A and thickness B with the rectangular scavenger particle of the length a and the thickness b (see Figure 4.16). The cell

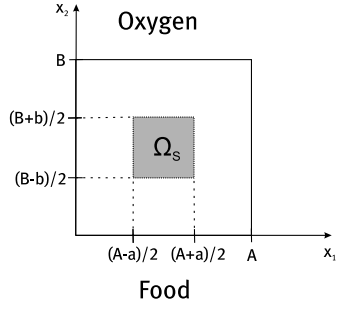

Figure 4.16: Cell with the scavenger particle in the center.

occupies the region $\Omega = \{\mathbf{x} \in \mathbb{R}^2 : 0 \leq x_1 \leq A,\ 0 \leq x_2 \leq B\}$ and the scavenger particle occupies $\Omega_s = \{\mathbf{x} \in \mathbb{R}^2 : (A-a)/2 \leq x_1 \leq (A+a)/2,\ (B-b)/2 \leq x_2 \leq (B+b)/2\}$. In the equations (4.2a)-(4.2b) we assume that $\alpha = \beta = 1$.

Therefore, the reaction-diffusion process in the cell is described by

$$\frac{\partial c(\mathbf{x},t)}{\partial t} = D\Delta c(\mathbf{x},t) - \kappa\, s(\mathbf{x},t)c(\mathbf{x},t), \tag{4.36a}$$

$$\frac{\partial s(\mathbf{x},t)}{\partial t} = -\kappa\, s(\mathbf{x},t)c(\mathbf{x},t), \tag{4.36b}$$

where $\mathbf{x} \in \Omega$ and $t \in [0,\infty)$. The initial concentration of oxygen in Ω is zero

$$c(\mathbf{x},0) = 0, \quad \mathbf{x} \in \Omega, \tag{4.37}$$

and the initial concentration of scavenger is s_0 in Ω_s and zero outside Ω_s.

$$s(\mathbf{x},0) = \begin{cases} s_0, & \mathbf{x} \in \Omega_s, \\ 0, & \mathbf{x} \in \Omega \setminus \Omega_s. \end{cases} \tag{4.38}$$

Because the concentrations of oxygen at both sides of the film are constant, we have Dirichlet boundary conditions for c at the top and bottom of the cell

$$c(\mathbf{x},t)|_{x_2=0} = 0, \quad c(\mathbf{x},t)|_{x_2=B} = c_a. \tag{4.39}$$

At the lateral sides of the cell we impose the periodic boundary condition

$$c(\mathbf{x},t)|_{x_1=0} = c(\mathbf{x},t)|_{x_1=A}, \quad \left.\frac{\partial c(\mathbf{x},t)}{\partial x_1}\right|_{x_1=0} = \left.\frac{\partial c(\mathbf{x},t)}{\partial x_1}\right|_{x_1=A}, \tag{4.40}$$

because the film consists of infinitely many cells.

We scale the distance x to the thickness, B, of the film, $\tilde{\mathbf{x}} = \mathbf{x}/B$, the time $\tilde{t} = tD/B^2$, the oxygen concentration as $\tilde{c} = c/c_a$, the scavenger concentration $\tilde{s} = s/c_a$ (here we assume that s and c have the same dimensions). After scaling the system (4.36a)-(4.40) becomes

$$\frac{\partial \tilde{c}(\tilde{\mathbf{x}},\tilde{t})}{\partial \tilde{t}} = \Delta\tilde{c}(\tilde{\mathbf{x}},\tilde{t}) - \tilde{\kappa}\,\tilde{s}(\tilde{\mathbf{x}},\tilde{t})\tilde{c}(\tilde{\mathbf{x}},\tilde{t}), \tag{4.41a}$$

$$\frac{\partial \tilde{s}(\tilde{\mathbf{x}},\tilde{t})}{\partial \tilde{t}} = -\tilde{\kappa}\,\tilde{s}(\tilde{\mathbf{x}},\tilde{t})\tilde{c}(\tilde{\mathbf{x}},\tilde{t}), \tag{4.41b}$$

$$\tilde{c}(\tilde{\mathbf{x}},0) = 0, \quad \tilde{\mathbf{x}} \in \tilde{\Omega}, \tag{4.41c}$$

$$\tilde{s}(\tilde{\mathbf{x}},0) = \begin{cases} \tilde{s}_0, & \tilde{\mathbf{x}} \in \tilde{\Omega}_s, \\ 0, & \tilde{\mathbf{x}} \in \tilde{\Omega} \setminus \tilde{\Omega}_s, \end{cases} \tag{4.41d}$$

$$\tilde{c}(\tilde{\mathbf{x}},\tilde{t})|_{\tilde{x}_2=0} = 0 \tag{4.41e}$$

$$\tilde{c}(\tilde{\mathbf{x}},\tilde{t})|_{\tilde{x}_2=1} = 1 \tag{4.41f}$$

$$\tilde{c}(\tilde{\mathbf{x}},\tilde{t})|_{\tilde{x}_1=0} = \tilde{c}(\tilde{\mathbf{x}},\tilde{t})|_{\tilde{x}_1=\tilde{A}}, \tag{4.41g}$$

$$\left.\frac{\partial \tilde{c}(\tilde{\mathbf{x}},\tilde{t})}{\partial \tilde{x}_1}\right|_{\tilde{x}_1=0} = \left.\frac{\partial \tilde{c}(\tilde{\mathbf{x}},\tilde{t})}{\partial \tilde{x}_1}\right|_{\tilde{x}_1=\tilde{A}}, \tag{4.41h}$$

for $\tilde{\mathbf{x}} \in \tilde{\Omega}$ and $\tilde{t} \in [0,\infty)$. Here $\tilde{A} = A/B$, $\tilde{a} = a/B$, $\tilde{b} = b/B$, $\tilde{\Omega} = \{\mathbf{x} \in \mathbb{R}^2 : 0 \le x_1 \le \tilde{A},\ 0 \le x_2 \le 1\}$, $\tilde{\Omega}_s = \{\mathbf{x} \in \mathbb{R}^2 : (\tilde{A}-\tilde{a})/2 \le x_1 \le (\tilde{A}+\tilde{a})/2,\ (1-\tilde{b})/2 \le$

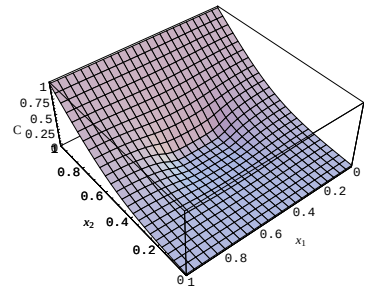

(a) Oxygen concentration at $t = 0.1$.

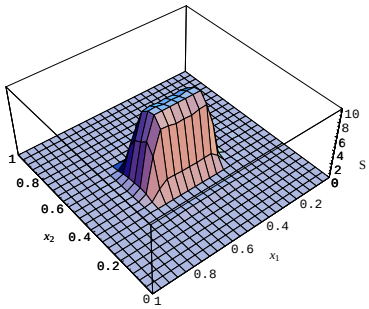

(b) Scavenger concentration at $t = 0.1$.

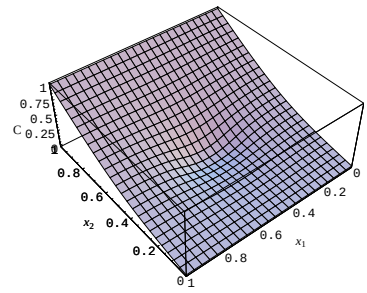

(c) Oxygen concentration at $t = 0.5$.

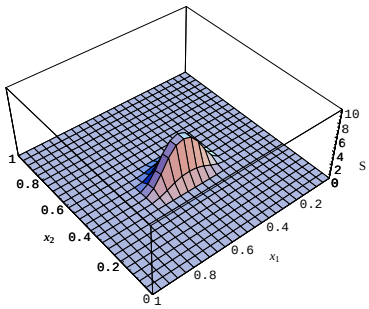

(d) Scavenger concentration at $t = 0.5$.

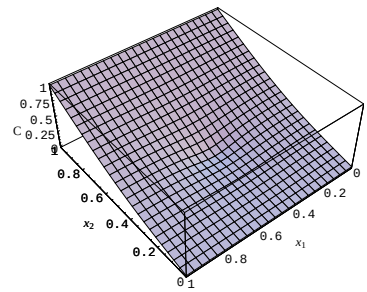

(e) Oxygen concentration at $t = 0.7$.

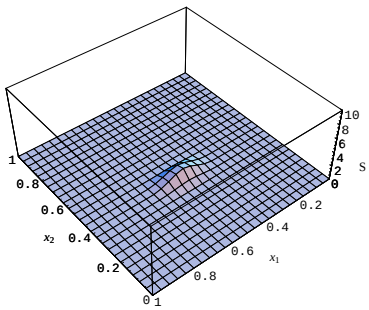

(f) Scavenger concentration at $t = 0.7$.

Figure 4.17: Concentrations of oxygen c and scavenger s in the cell at times $t = 0.1$, $t = 0.5$ and $t = 0.7$ for $a = 0.4$ and $b = 0.25$.

$x_2 \leq (1+\tilde{b})/2\}$, $\tilde{\kappa} = \kappa c_a B^2/D$ and $\tilde{s}_0 = s_0/c_a$. In the following we omit the tildes.

The system (4.41a)-(4.41h) is solved numerically in Mathematica for $\kappa = 100$, $s_0 = 10$ and $A = 1$. We vary the shape of the scavenger particle while the area remains constant, $ab = 0.1$, because the scavenger occupies 10% of the film. In Figure 4.17 we present the oxygen concentrations and the scavenger concentrations in the cell at times $t = 0.1$, $t = 0.5$ and $t = 0.7$. The size of the scavenger particle is taken to be $a = 0.4$, $b = 0.25$. When the scavenger disappears the oxygen profile becomes more straight.

For a real application it is important to know a flux through the film. We compute the flux through the cell as

$$F(t) = -\int_0^A \frac{\partial c(x_1, 0, t)}{\partial x_2} dx_1. \tag{4.42}$$

In Figure 4.18 we present the flux for different sizes of the scavenger particle (see Figure 4.19) as a function of time. If the length of the scavenger particle

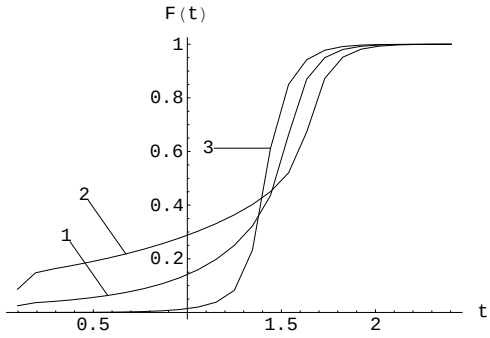

Figure 4.18: Flux through the cell for different sizes of the scavenger particle (line 1 $a = 0.6666$, $b = 0.15$; line 2 $a = 0.3162$, $b = 0.3162$; line 3 $a = 1$, $b = 0.1$).

is equal to the length of the cell (line 3) then the short time behavior is better than that for the droplets with other shapes. But after the scavenger disappears the flux becomes large, while the droplets with the other shapes (lines 1 and 2) still react with the oxygen. If the scavenger particle has a square shape (line 2) then it reacts longer than the droplets with the other rectangular shapes. The flux of a square scavenger droplet is initially larger than that of scavenger droplets with other rectangular shapes.

4.8 Conclusions

This Study Group turned out to be an inspiring and creative week. Not only is this our perception as a group, but it also comes forward in the scientific

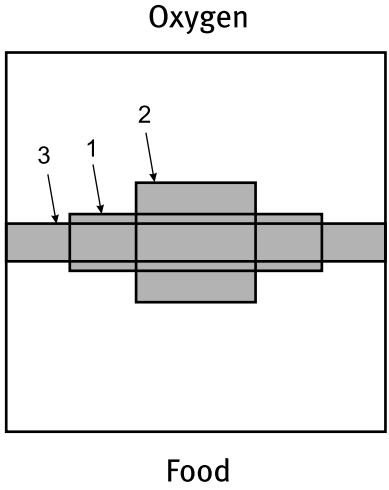

Figure 4.19: Different shapes of the scavenger particle (line 1 $a = 0.6666$, $b = 0.15$; line 2 $a = 0.3162$, $b = 0.3162$; line 3 $a = 1$, $b = 0.1$).

contents (and size!) of this report and the various approaches that are proposed within. The fruitful cooperation is moreover underlined by the large number of authors who were willing to contribute, and the number of people that helped us during the week. Different approaches were discussed critically, with the result that only a small part of the ideas coined were found to be worth reporting. These approaches cover methods, techniques and ideas about three general areas: the modelling (section 4.2), the analysis (section 4.3, 4.4 and 4.5), and numerical simulations (section 4.6 and 4.7). We give a short summary of the conclusions that we have drawn.

The stochastic model that is derived in section 4.2 converges in a weak sense to the model proposed by DSM. In section 4.3 it is concluded that for very small length scales and for small amounts of scavenger, thin, elongated droplets are more effective than small spherical droplets. In section 4.4 it is shown that, in the one-dimensional case, the penetration time of oxygen through the foil depends quadratically on the diameter of scavenger particles, and linearly on the amount of scavenger, and linearly on the distance between the particles and the outside surface of the foil. In section 4.5 it is concluded that in order to investigate the influence of droplet shapes, the DSM model can be converted via conformal mappings to a set of equations that are more attractive numerically and analytically. One-dimensional simulations in section 4.6 show that two small homogeneously distributed droplets are more effective than one big droplet. Finally, two-dimensional simulations in section 4.7 show that cigar- and pancake-shaped droplets perform better than spherical droplets initially, but that then the scavenger reacts away faster.

The problem owners from DSM, prof. dr. Han Slot, and dr. Alexander Stroeks were very clear in their explanation and motivation of the problem, which helped us work in the most interesting directions, mathematically as well as practically. We do hope that the mathematical insight we developed and reported, will provide guidelines in ways of solving their problems.

4.9 Acknowledgement

We acknowledge the input and time of Alexander Stroeks and Han Slot from DSM and the work of all the participants in the DSM group and the people from outside our group who helped by supplying new ideas: Hala Elrofai, Vincent Guyonne, Joost Hulshof, Vivi Rottschäfer, Martin van der Schans, Paul Zegeling, Geertje Hek, Remco van der Hofstad, and Matthias Röger.

4.10 Bibliography

[1] D. Hilhorst, R. van der Hout, and L. A. Peletier. The fast reaction limit for a reaction-diffusion system. *J. Math. Anal. Appl.*, 199(2):349–373, 1996.

[2] U. Hornung. *Homogenization and Porous Media*. Springer-Verlag, Berlin, 1996.

[3] L.P.B.M. Janssen J.M.Smit, E. Stammers. *Fysische Transportverschijnselen I*, volume III. Delft University Press, 6 edition, 1973.

[4] Landim C. Kipnis C. *Scaling limits of interacting particle systems*. Springer, Berlin, 1999.

[5] T.M. Liggett. *Interacting particle systems*. Springer, New York, 1985.

[6] Z. Nehari. *Conformal Mapping*. McGraw-Hill, New York, 1952.